Small Centrifugal Pumps for Low-Thrust Rockets

R.B. Furst,* R.M. Burgess,† and N.C. Gulbrandsen‡
Rockwell International/Rocketdyne Division, Canoga Park, California
and
D.D. Scheer§
NASA Lewis Research Center, Cleveland, Ohio

The objective of the investigation is to evaluate analytically and experimentally small-diameter, very low specific-speed centrifugal pumps for potential use as components of propellant feed systems for low-thrust rocket engines. Six pumps were designed, fabricated, and tested by pumping water. Both fully shrouded and open-face impellers were evaluated at design-specific speeds (dimensionless) [(rpm)(gpm)$^{0.5}$ (ft)$^{-0.75}$] of 0.158 (430) and 0.079 (215). At the 0.158 (430) specific speed, design point efficiency for the fully shrouded impellers was approximately 30% and, at the 0.079 (215) specific-speed design point, 10%. The efficiency of the open-face impeller pumps was substantially lower than for the fully shrouded impeller pumps. Partial-emission diffusers were found to permit larger impeller and diffuser passages with a minimal performance difference at the same specific speed. The same impeller was operated at design point flow-rate ratios of 4 to 1 by use of partial-emission diffusers. The suction performance of the 2-in.-diam impellers was typical of those for normal commercial pumps, and standard prediction procedures for large-diameter pumps were proved to be adequate.

Nomenclature

admission = $\dfrac{\text{impeller inlet free annulus area}}{\text{total impeller inlet annulus area}}$

C_{m1}, C_{m2} = impeller inlet and exit meridional velocities, respectively

emission = $\dfrac{\text{diffuser free inlet annulus area}}{\text{total diffuser inlet annulus area}}$

g = gravitational constant, consistent units

H = overall pump head, m (ft)

N_s = specific speed $\dfrac{\omega Q^{0.5}}{(g\,H)^{0.75}}\left[\dfrac{\text{rpm}\ Q^{0.5}}{H^{0.75}}\right]$

Q = inlet volume flow rate, m^3/s (gal/min)

S_s = suction specific speed $\dfrac{\omega Q^{0.5}}{(g\ \text{NPSH})^{0.75}}$, $\left[\dfrac{\text{rpm}\ Q^{0.5}}{\text{NPSH}^{0.75}}\right]$

U_1, U_2 = impeller inlet and discharge peripheral velocities, respectively

ϕ_1 = impeller inlet flow coefficient, C_{m1}/U_1, dimensionless

ϕ_2 = impeller discharge flow coefficient, C_{m2}/U_2

ψ = pump overall head coefficient, gH/U_2^2

ω = rotational speed, rad/s

Received June 21, 1985; presented as Paper 85-1302 at the AIAA/SAE/ASME/ASEE 21st Joint Propulsion Conference, Monterey, CA, July 8-10, 1985; revision received Aug. 8, 1986.
Copyright © American Institute of Aeronautics and Astronautics, Inc., 1987. All rights reserved.

*Manager, Hydrodynamics.
†Member Technical Staff.
‡Manager, Technology Projects. Member AIAA.
§Project Manager.

Introduction

PUMP-FED, low-thrust chemical propulsion systems are being considered for transferring acceleration limited structures from low-Earth orbit to geosynchronous or other high-Earth orbits. Engine systems for these applications will require small, relatively low flow-rate, high head rise pumps that fall outside the design range of existing rocket engine turbopumps. To establish a technology base for future design of these systems, a program was initiated to experimentally evaluate low specific-speed centrifugal pump stages over the flow-rate range of interest. The test program was structured to determine performance of each of the six centrifugal stages, with water as the test fluid.[1]

This paper discusses design of the centrifugal stages and presents the water test performance results. Also included is a comparison of predicted losses for the two stages that are to be tested pumping liquid hydrogen.

Pump Configurations

Design

Six centrifugal pump configurations were designed and tested and are listed in Table 1. Four configurations were designed for a specific speed, $N_s = 0.158$ (430). These pumps were designated configurations 1, 2, 4, and 6 (Table 2). All pump configurations incorporated impellers with an axial inlet and a radial discharge.

Configurations 3 and 5 were designed for $N_s = 0.079$ for (215) (Table 2). All pumps incorporated impellers with 50.8-mm (2-in.) tip diameters. Configurations 1-3 utilized the same shrouded impeller. The differences between test and design wear-ring clearances (Tables 1 and 2) are due to opening of the clearance to prevent rubbing during operation.

The tip widths of all the impellers are very small (Table 2) because of the low specific speed, even though the discharge flow coefficient is lower than normal.[2]

Configuration 1, listed in Table 2, incorporates a 100% admission shrouded impeller discharging into a 100% emission vaned diffuser, which discharges into a volute. The impeller is fully shrouded with backward-curved blades. The vaned diffuser is the vane island type with eight straight mean line diffusing passages machined into the inlet housing rear face. To reduce friction loss, the volute is designed with

Table 1 Low-thrust rocket engine centrifugal pump test configurations

Configuration	Impeller type	Diffuser type	Front wear-ring radial clearance, mm (in.)	Rear wear-ring axial clearance, mm (in.)	Face axial clearance, mm (in.)	Impeller tip width, mm (in.)
1	Shrouded 100% admission	Vaned 100% emission	0.0381 (0.0015)	0.0508 (0.0020)	—	0.762 (0.030)
2	Shrouded 100% admission	Volute exit	0.0635 (0.0025)	0.0508 (0.0020)	—	0.762 (0.030)
3	Shrouded 100% admission	Vaned 25% emission	0.0660 (0.0026)	0.0508 (0.0020)	—	0.762 (0.030)
4	Open-face 100% admission	Volute exit	—	0.114 (0.0045)	0.254 (0.010)	0.889 (0.035)
5	Open-face 25% admission	Volute exit	—	0.0965 (0.0038)	0.203 (0.008)	0.889 (0.035)
6	Shrouded 100% admission	Vaned 50% emission	0.0787 (0.0031)	0.0762 (0.0030)	—	1.32 (0.052)

Table 2 Pump design geometry

	Configuration					
	1	2	3	4	5	6
Pump specific speed	430	430	215	430	215	430
Speed, rpm						
Water	24,500	24,500	39,200	24,500	39,200	24,500
Liquid hydrogen	77,000	77,000	125,000	77,000	125,000	77,000
Flow, m^3 (gpm)						
Water	3.16×10^{-4}(5.0)	3.16×10^{-4}(5.0)	1.26×10^{-4}(2.00)	3.16×10^{-4}(5.0)	1.26×10^{-4}(2.00)	3.16×10^{-4}(5.0)
Liquid hydrogen	9.91×10^{-4}(15.7)	9.91×10^{-4}(15.7)	4.33×10^{-4}(6.87)	9.91×10^{-4}(15.7)	4.33×10^{-4}(6.87)	9.91×10^{-4}(15.7)
Head, m (ft)						
Water	194 (637)	194 (637)	497 (1630)	194 (637)	521.6 (1711)	194 (637)
Hydrogen	1921 (6300)	1921 (6300)	5061 (16,000)	1921 (6300)	5530 (18,140)	1921 (6300)
Impeller						
Type	Shrouded	Shrouded	Shrouded	Open-face	Open-face	Shrouded
Discharge diameter, mm (in.)	50.8 (2.0)	50.8 (2.0)	50.8 (2.0)	50.8 (2.0)	50.8 (2.0)	50.8 (2.0)
Inlet eye diameter, mm (in.)	19.05 (0.75)	29.05 (0.75)	19.05 (0.75)	20.32 (0.80)	20.32 (0.80)	20.51 (0.81)
Inlet hub diameter, mm (in.)	12.7 (0.50)	12.7 (0.50)	12.7 (0.50)	12.7 (0.50)	12.7 (0.50)	12.7 (0.50)
Discharge tip width, mm (in.)	0.762 (0.030)	0.762 (0.030)	0.762 (0.030)	0889 (0.035)	0.889 (0.035)	1.32 (0.052)
Number of blades	7	7	7	8	2	7
Discharge blade angle, deg	33	33	33	20	20	33
Impeller face clearance, mm (in.)	—	—	—	0.012 (0.004)	0.1016 (0.004)	—
Front wear-ring radial clearance, mm (in.)	0.0254 to 0.0508 (0.001 to 0.002)	0.0254 to 0.0508 (0.001 to 0.002)	0.0254 to 0.0508 (0.001 to 0.002)	— —	— —	0.0254 to 0.0508 (0.001 to 0.002)
Rear wear-ring radial clearance, mm (in.)	0.0254 to 0.0508 (0.001 to 0.002)	0.0254 to 0.0508 (0.001 to 0.002)	0.0254 to 0.0508 (0.001 to 0.002)	0.0254 to 0.0508 (0.001 to 0.002)	0.0254 to 0.0508 (0.001 to 0.002)	0.0254 to 0.0508 (0.001 to 0.002)
Inlet eye blade angle, deg	21.9	21.9	21.9	21.25	21.25	20
Inlet flow coefficient (10% blockage)	0.134	0.134	0.134	0.1	0.107	0.174
Percent admission	100	100	100	100	25	100
Discharge flow coefficient	0.074	0.074	0.074	0.080	0.080	0.085
Diffuser (inlet)						
Inlet diameter, mm (in.)	53.4 (2.1)	—	53.4 (2.1)	—	—	53.4 (2.1)
Discharge diameter, mm (in.)	68.6 (2.7)	—	68.6 (2.7)	—	—	68.6 (2.7)
Passage width, mm (in.)	0.762 (0.030)	—	0.762 (0.030)	—	—	1.32 (0.052)
Number of passages	8	—	2	—	—	4
Inlet angle, deg	6	—	6	—	—	6
Area ratio, out/in	1.84	—	1.84	—	—	1.84
Percent emission	100	—	25	—	—	50
Volute						
Maximum area at 360 deg, m^2 $(in.)^2$	3.02×10^{-5} (0.0468)	1.72×10^{-5} (0.0267)	9.43×10^{-6} (0.0146)	2.26×10^{-5} (0.035)	7.1×10^{-6} (0.011)	3.02×10^{-5} (0.0468)
Continuity area/actual area	0.60	0.60	0.50	0.83	0.833	0.60
Conical diffuser exit area, m^2 $(in.^2)$	6.2×10^{-5} (0.096)	6.2×10^{-5} (0.096)	6.2×10^{-5} (0.096)	6.2×10^{-5} (0.096)	1.68×10^{-5} (0.026)	6.2×10^{-5} (0.096)

proportionately larger cross-section area than for a large, higher specific-speed pump. The area distribution is designed to minimize radial load through equalizing static pressure circumferentially. The use of a vaned diffuser produces a nearly constant radial load over a wide flow range since the diffuser produces a volute velocity matching the flow rate down to the diffuser stall flow rate.[3]

Configuration 2 listed in Table 2 utilizes the same impeller as configuration 1 but discharges its flow directly into a volute. Diffusion is accomplished by a volute exit conical diffuser.

Configuration 3 utilizes the same impeller as configurations 1 and 2. The impeller discharges through a 25% emission diffuser, which has the same diffuser passage geometry as configuration 1. The diffuser differs in that only two opposite passages were machined, compared to eight for configuration 1. The intent is to reduce the design flow rate to one-fourth at the same operating speed and the specific

speed to one-half of that for a 100% emission diffuser (Table 2).

Configuration 4 incorporates an open-face impeller with 100% admission, which discharges directly into a volute. The diffusion is accomplished by a conical diffuser at the volute exit (Table 2).

Configuration 5 incorporates a 25% admission open-face impeller that discharges directly into a volute shaped to minimize dynamic radial loads. The impeller passage geometry is the same as for configuration 4. The impeller geometry differs in that only two opposite passages are machined as compared with eight for configuration 4. This modification was intended to reduce the design flow rate to one-fourth that of a 100% admission impeller (Table 2).

Configuration 6 incorporates a 100% admission shrouded impeller with the same blade shape as for configurations 1-3, except that the impeller passage height is increased from inlet to exit. The impeller discharges into a 50% emission vaned diffuser with increased passage height but otherwise the same passage shape as for configurations 1-3. This configuration is intended to operate at the same design point flow as configuration 1. The larger flow passages were used to simplify fabrication (Table 2).

Analysis of Pump Losses

After completion of the water test program, configurations 2 and 6 were selected for further tests and will be tested with liquid hydrogen as the pumped fluid. Predicted losses for these configurations when water or liquid hydrogen is pumped are given in Table 3. The losses presented are a percentage of the total power input. The types of loss noted in the tables are typical of those considered in performance prediction of pumps incorporating shrouded impellers.

Partial-emission pump performance was evaluated, assuming that the flow velocity in the flowing impeller passages was equal to the impeller through-flow divided by the percent emission plus wear-ring leakage flow. This fluid quantity was then used to calculate impeller friction diffusion and incidence loss in the flowing passages. No unsteady flow loss was computed and, because this loss is largely a function of the impeller exit radial velocity and with the low impeller flow coefficient for these low specific-speed pumps, this loss is small. For higher specific-speed pumps and compressors with higher impeller passage velocities, this loss would be significant.[2,4]

Comparison of results for pumping water with results for pumping liquid hydrogen (Table 3) shows that flow friction and, in particular, disk friction losses are significantly lower when pumping liquid hydrogen. This is due to the much lower viscosity of hydrogen and results in higher efficiency. The losses associated with leakage, diffusion, and momentum are a higher percentage of the power input as a result of the reduced input power resulting from the lower disk friction. Analytical procedures similar to those used in analyzing the pump performance are presented in Ref. 2.

By far the highest individiual losses in either fluid are the disk friction loss and the impeller wear-ring (seal) leakage loss. With wear-ring radial clearances of only 0.002 in., the total of these two losses accounts for approximately 47% of total power input when pumping water and 41 percent when pumping liquid hydrogen. With low specific-speed pumps, the clearance must be small to reduce leakage loss. This is illustrated in Table 3, which shows the influence of a clearance change on configuration 6 when pumping liquid hydrogen. An increase in radial clearance from 0.002 to 0.003 in. results in a decrease in predicted efficiency from 40.4 to 35.4%, which would require a 14% increase in input power.

The leakage loss for the shrouded impellers includes the front (impeller inlet) and rear wear-ring flows. The rear wear-ring flow is returned to the impeller inlet through passages in the housing, which remove any tangential velocity component. The leakage flow through the impeller inlet wear ring, however, has a tangential velocity approximately equal to half the wheel speed at the impeller inlet prior to mixing with the incoming flow. This tangential velocity produces prewhirl at the impeller inlet, which drops the change of angular momentum produced by the impeller and therefore reduces the pump head rise. As the delivered pump flow is reduced from its normal operating flow rate, the ratio of the impeller total flow to the whirling front wear-ring flow is decreased. This results in increasing prewhirl as the flow is reduced. The increased prewhirl acts to reduce pump head rise at reduced delivered flow while the increased tangential velocity at the backward-curved impeller blade exit acts to increase the pump heat rise. The result at low specific speeds is a nearly constant heat rise with charging delivered flow which agrees well with test pressure.

Test Program

Facility Description

The water test program was conducted in a specially constructed small pump test facility. The test facility was capa-

Table 3 Predicted losses percent of input power

	Pumping water		Pumping liquid hydrogen		
Pump configuration	2	6	2	6	
Speed, rpm	24,500	24,500	77,000	77,000	
Flow rate, m^3/s (gpm)	3.16×10^{-4}(5.0)	3.16×10^{-4}(5.0)	9.91×10^{-4}(15.7)	9.91×10^{-4}(15.7)	
Wear-ring clearance, mm (in.)	0.0508 (0.002)	0.0508 (0.002)	0.0508 (0.002)	0.0508 (0.002)	0.0762 (0.003)
Total wear-ring clearance	23.9	25.2	27	28.3	37.4
Disk friction	23.3	21.2	14.4	13.0	11.7
Impeller internal friction	5.69	4.02	5.4	3.4	3.3
Impeller diffusion	0.98	2.3	1.36	2.5	1.82
Impeller incidence	0.50	0.51	0.56	0.56	0.41
Impeller exit recirculation	0	0.34	0	03.34	0.03
Vaneless space friction	0.90	0.84	0.8	0.79	0.57
Vaned diffuser incidence	—	1.38	0	1.55	1.28
Vaned diffuser friction	—	2.79	—	2.40	2.06
Vaned Diffuser diffusion	—	4.62	—	5.08	4.52
Volute momentum	1.44	0.15	1.65	0.14	0.16
Volute friction	3.99	1.77	3.48	1.45	1.33
Volute diffusion	0.27	0.07	0.3	0.08	0.07
Total	60.97	65.2	55.0	59.6	64.6
Predicted efficiency	39.03	34.8	55.0	40.4	35.4
Corrected test efficiency	34.9	30.9	—	—	—

ble of conducting tests over a wide range of speed, flow, and inlet pressures.

The facility includes a closed-circuit pump flow loop with pressure level control and a turbine gaseous nitrogen (GN_2) supply and exhaust system. The pump inlet pressure can be lowered by dropping the water tank pressure by means of a vacuum source or increased by pressurizing the tank with gaseous nitrogen. The test pumps are installed in the pump tester and driven by an axial flow turbine. The pump/tester cross section is shown in Fig. 1. Typical pump instrumentation is shown in Fig. 2. All instrumentation was calibrated by standards traceable to the Bureau of Standards prior to testing of each pump configuration. Calibrations were checked pre- and posttest.

Test Procedures

The tests evaluated head rise vs flow rate at target speeds of 24,500, 19,600, 14,700, and 7350 rpm for configurations 1, 2, 4, and 6 and at target speeds of 31,360, 23,520, and 11,760 rpm for configurations 3 and 5. The head rise was measured by the difference in pressure between the four-hole static pressure piezometer ring located 5 diameters upstream of the pump inlet (±0.5 psi) and the four-hole static pressure piezometer ring located 10 diameters downstream of the pump discharge (±2.5 psi). The pump flow rate was measured by means of a flowmeter (±0.5%) located in the pump discharge line. The flow rate was controlled by a valve located downstream of the flowmeter in the same line. Pump speed (±0.5%) was controlled by varying the turbine inlet and discharge pressure to control the power input to the pump.

Sufficient pressure measurements were made in the pump to permit calculation of the pump axial and radial loads and internal performance at test operating conditions.

Suction performance tests were conducted by operation at a constant pump rotating speed and flow rate with the pump inlet pressure gradually lowered from a high to a low value. Vapor pressure was determined from measured temperature (±0.2 R). The higher test speeds produced consistent suction specific-speed values and were therefore used to determine the pump suction performance. Suction performance data were not obtained for configuration 1 due to damage to the volute wear-ring during the head vs flow test. Since the same impeller was used for configuration 2, the suction performance capability of the impeller was evaluated by test of configuration 2.

The pump power was determined by computing the power generated by the drive turbine based on test measurements and turbine calibration data. The turbine was calibrated after the pump test program using a Kahn water dynamometer. Power available to the pump was determined by connecting the turbine mounted on the pump tester to the dynamometer. The turbine was driven by dry gaseous nitrogen during calibration. Turbine measurements during calibration were the same as those obtained during the pump tests to provide a direct relationship of calibration information. The dynamometer replaced the pump as the power absorber. Therefore, the turbine calibration included the rotating assembly bearing and seal power losses up to the pump and the Kahn dynamometer absorbed horsepower was directly the pump input horsepower.

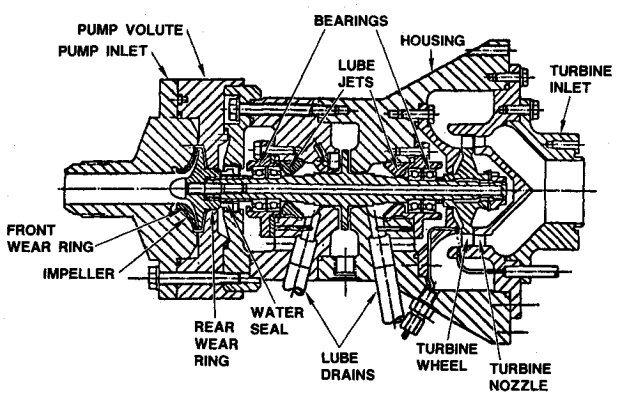

Fig. 1 Pump/tester cross section.

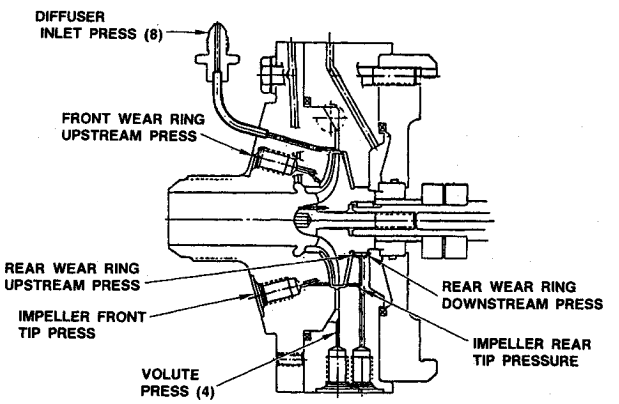

Fig. 2 Typical pump instrumentation.

Test Results

Head and Efficiency vs Flow

Table 4 summarizes the pump design point head and efficiency at the design point flow rates, while Figs. 3–6 present the head, flow, and efficiency data for the shrouded impeller configurations (1, 2, 3, and 6). Test data from open-faced configurations 4 and 5 are included (Figs. 7 and 8) but not discussed due to unrepresentative performance caused by operation with above design value impeller blade clearance. The wear-ring radial clearances and open-face impeller axial clearances are listed in Table 2.

Pump configurations 1, 2, and 6 were designed to operate at a design point specific speed (N_s) of 0.158 (430). The highest design point efficiency (32.5%) and head rise [228.7 m (750 ft) at 24,500 rpm] was achieved by configuration 2,

Table 4 Design point performance summary

Test configuration	Test shaft speed, rpm	Flow rate, m^3/s (gpm)	Test head, m (ft)	Percent efficiency		Inlet NPSH at 5% head falloff, m (ft)	Suction[b] specific speeds (S_s), test	Suction[b] specific speed (predicted)	$\frac{S_s \text{ (Test)}}{S_s \text{ (Pred)}}$
				Test	Corrected[a]				
1	24,500	3.16×10^{-4} (5.0)	221 (725)	31.0	30.1	3.35 (11.6)	3.18 (8,700)	3.38 (9,235)	0.94
2	24,500	3.16×10^{-4} (5.0)	229 (750)	32.5	33.5	3.35 (11.6)	3.18 (8,700)	3.43 (9,370)	0.93
3	29,000	9.35×10^{-5} (1.48)	344 (1130)	9.6	11.2	2.04 (6.7)	2.85 (7,800)	1.59 (4,345)	1.80
4	24,500	3.16×10^{-4} (5.0)	136 (445)	23.0	—	2.68 (8.8)	3.92 (10,700)	2.72 (7,440)	1.44
5	29,000	9.35×10^{-5} (1.48)	104 (342)	5.1	—	4.02 (13.2)	1.87 (5,100)	1.60 (4,370)	1.17
6	24,500	3.16×10^{-4} (5.0)	227 (745)	28.5	32.9	3.29 (10.8)	3.25 (8,600)	2.61 (7,120)	1.29

[a]Corrected to 0.002-in. radial wear-ring clearance. [b]Dimensionless ($rpm \times gpm^{0.05} \times ft^{-0.75}$).

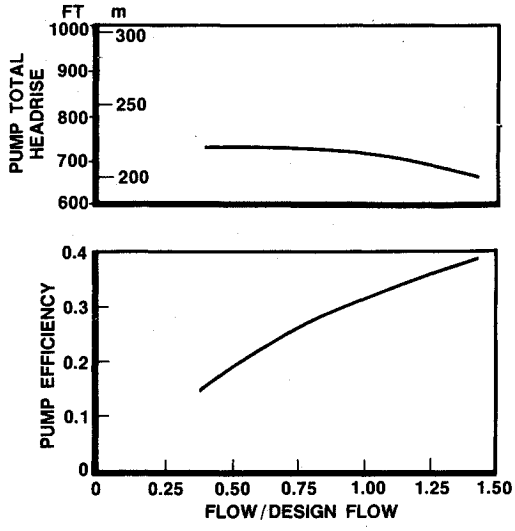

Fig. 3 Low-thrust pump configuration 1 ($N = 24{,}500$ rpm, $N_s = 430$).

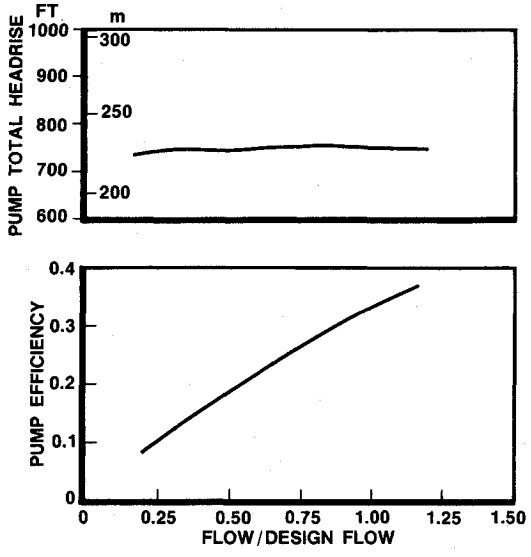

Fig. 4 Low-thrust pump configuration 2 ($N = 24{,}500$ rpm, $N_s = 430$).

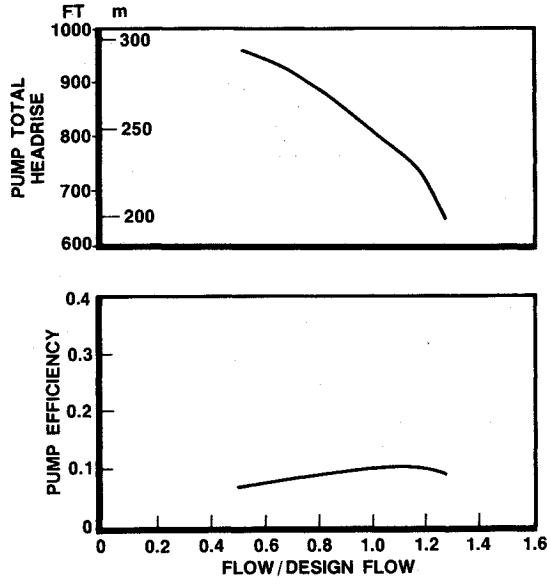

Fig. 5 Low-thrust pump configuration 3 ($N = 24{,}500$ rpm, $N_s = 215$).

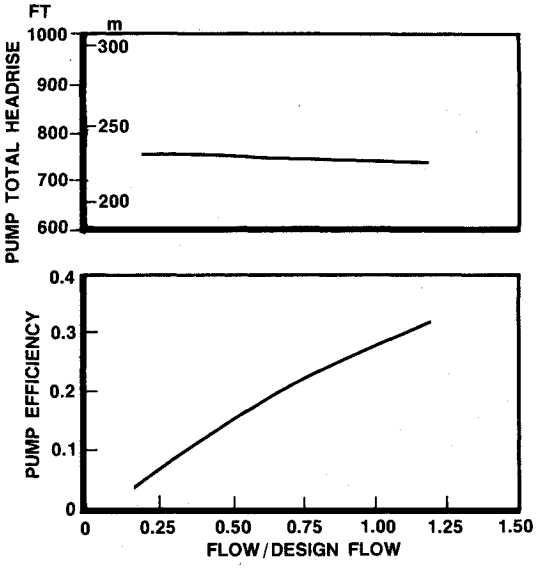

Fig. 6 Low-thrust pump configuration 6 ($N = 24{,}500$ rpm, $N_s = 430$).

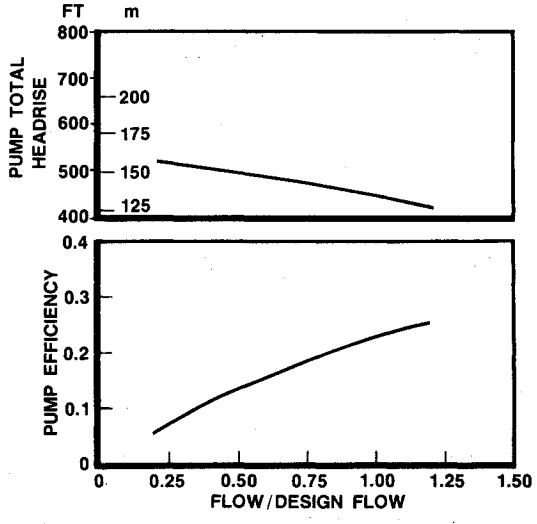

Fig. 7 Low-thrust pump configuration 4 ($N = 24{,}500$ rpm, $N_s = 430$).

which utilized a shrouded impeller with a 0.762-mm (0.030-in.) exit tip width discharging into a volute with a conical diffuser at the exit. The lowest efficiency (23%) and head rise [135.7 m (445 ft)] of the four configurations was produced by configuration 4, which was similar to configuration 2 except for the use of an open-face impeller rather than a shrouded impeller. The second-highest efficiency (31%) and third-highest head rise [221 m (725 ft)] was achieved by configuration 1, which used the same impeller as configuration 2 but which discharged through a vaned diffuser followed by a volute and exit diffuser. The third-highest efficiency (28.5%) and second-highest head rise [227 m (745 ft)] was achieved by configuration 6, which used a shrouded impeller with a 1.32-mm (0.052-in.) exit tip width discharging through a 50% emission vaned diffuser into a volute. The head rise and efficiency results are influenced by the wear-ring clearances and the axial clearance of the open-face impeller. Test configuration 1 operated with wear-ring clearances within the pretest design values, while the other configurations were tested with clearances that were slightly larger than design (Tables 1 and 2) to avoid rubbing. The efficiencies would have been higher if the pumps had been operated with the design clearances. Configuration 6 efficiency was better than configuration 1, based on corrected

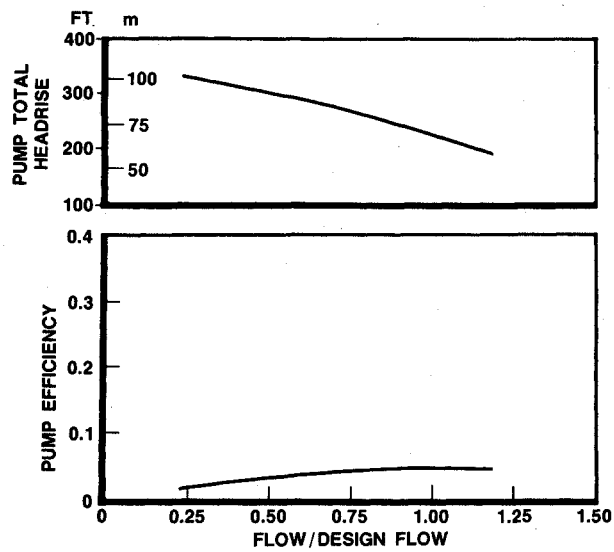

Fig. 8 Low-thrust pump configuration 5 ($N = 24{,}500$ rpm, $N_s = 215$).

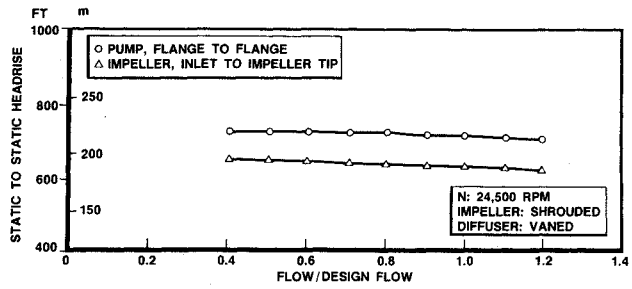

Fig. 9 Pump and impeller static head rise (low-thrust centrifugal stage, configuration 1).

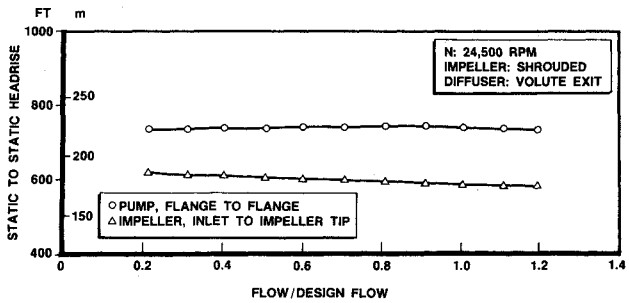

Fig. 10 Pump and impeller static head rise (low-thrust centrifugal stage, configuration 2).

efficiency, thus indicating the potential of partial emission pumps for low specific speeds.

Configurations 3 and 5 were designed to opeate at a design point specific speed of 0.079 (215). At the test speed of 29,000 rpm, configuration 3 achieved the higher efficiency of 9.6% and head of 344 m (1130 ft). This configuration incorporated the same shrouded impeller as configurations 1 and 2 and discharged through a 25% emission diffuser and volute. The low efficiency of configurations 3 and 5 result from the very low flow rate, one-fourth that of configurations 1, 2, and 6, at the same speed. At one-fourth the delivered flow, the hydraulic power output is reduced to one-fourth. The input power, however, is only slightly reduced, resulting in the low efficiency.

The efficiency correction for clearance variation is based on calculated wear-ring leakage rates and calculated disk friction values.[2] It was assumed that the disk friction did not

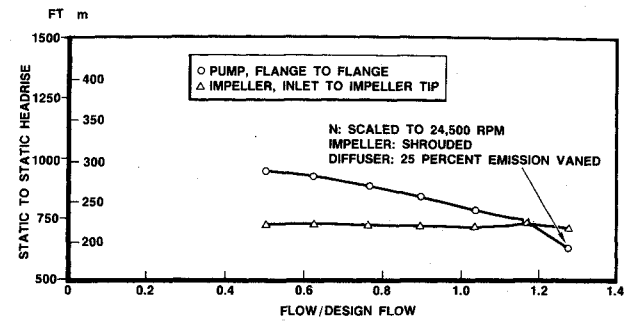

Fig. 11 Pump and impeller static head rise (low-thrust centrifugal stage, configuration 3).

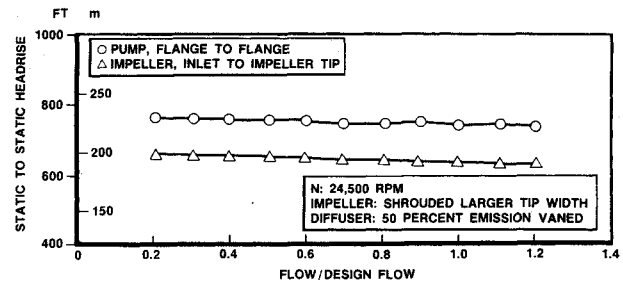

Fig. 12 Pump and impeller static head rise (low-thrust centrifugal stage, configuration 6).

change as the leakage flow was changed, although a small variation is to be expected.

Comparison of the impeller static pressure rise and the overall pump static pressure rise is a measure of the ability of the diffuser system to convert impeller exit velocity head to static pressure. Figures 9–12 show that configuration 2, with the vaneless conical diffuser, recovered the most velocity head. Configuration 2, as well as the vaned configurations 1 and 6, were not affected by changes in flow rate. The 25% emission vaned diffuser configuration 3, however, was affected: its ability to recover velocity head declined as the flow rate was increased. Table 5 summarizes the design point diffuser system performance. Configuration 2 with the vaneless conical diffuser appears to be the most desirable, with its superior performance and simplicity leading to low cost.

Suction Performance

Cavitation tests were run at constant pump speed and flow rate for pump configurations 2–6. Pump configuration 1 was not run because it contains the same impeller as configuration 2 and therefore would have the same suction performance. Only the data for the highest test speed are presented since they are the most accurate. All suction performance data are presented at 5% overall pump head loss. The design point predicted and test suction performance are compared for the six configurations in Table 4. The test and predicted suction performance compare closely except for configurations 3 and 4, which exceeded predicted suction specific speed by 80 and 44%, respectively. It is apparent that the degree of conservatism applied to account for inlet flow recirculation for configurations 3 and 4 was greater than necessary.

The configuration 2 pump total head rise NPSH showed that its head rise is constant over a wide NPSH range for flow rate. The suction specific speed vs flow ratio for configurations 1, 2, 3, and 6 is shown in Fig. 13. Configurations 4 and 5 are shown in Fig. 14.

The head rise vs NPSH is constant for configuration 3 over a wide NPSH range at 80 and 100% of the design flow

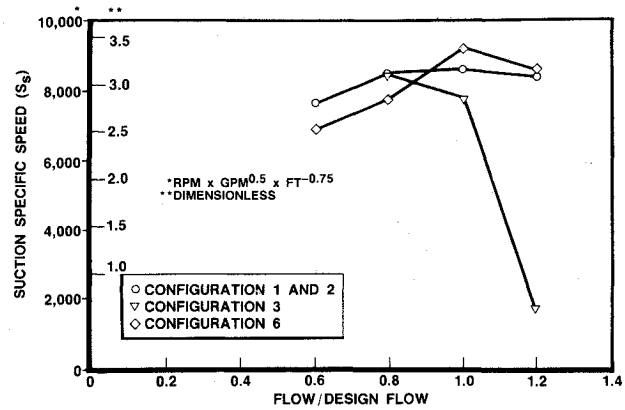

Fig. 13 Low-thrust pump, shrouded impellers (suction performance).

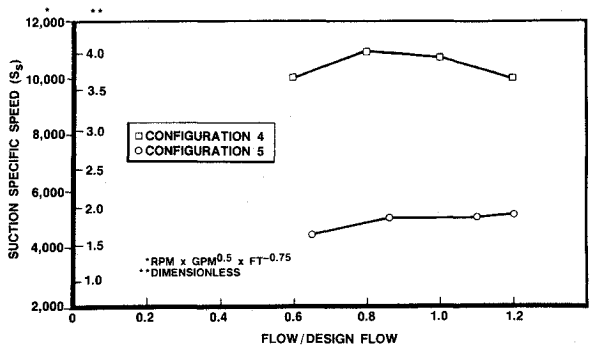

Fig. 14 Low-thrust pump, open-face impellers (suction performance).

rate. At 120% of design flow rate, the head rise begins to drop as NPSH is decreased below approximately 30.5 m (100 ft) at 27,440 test rpm. The test results presented in Fig. 11 indicate that the diffuser static pressure recovery continuously decreases as the flow rate is increased, until at 120% of design flow rate the recovery is zero. This, along with the low suction specific speed capability at 120% flow, indicates the vaned diffuser may be cavitating (Fig. 13). This may be a function of the percent emission since the 50% emission configuration 6 demonstrated a constant head rise over a wide flow range as well as a constant diffusing system static pressure rise over a wide flow range.

Configuration 6 head vs NPSH for the flow ratios of 0.8, 1.0, and 1.2 showed that constant head was generated over a wide NPSH range for the three flow rates.

The predicted cavitation performance (Table 4) at the design point is based on the procedure developed by Gongwer and presented by Wislicenus.[6] For the partial admission and emission pumps, the impeller inlet area was determined by multiplying the geometric area by emission or admission ratio.

The calculated leakage flow rate was added to the through-flow rate in computing the impeller flow rate to determine the impeller inlet flow coefficient.

Hydrodynamic Shaft Loading

Each pump was instrumented to measure pressures required to calculate radial and axial forces produced by the impeller.

Radial Load

The radial loads are determined from the static pressure distribution downstream of the impeller. For the vaned diffuser pumps the static pressure taps are located in the diffuser passage inlet. The number of diffuser passages, and

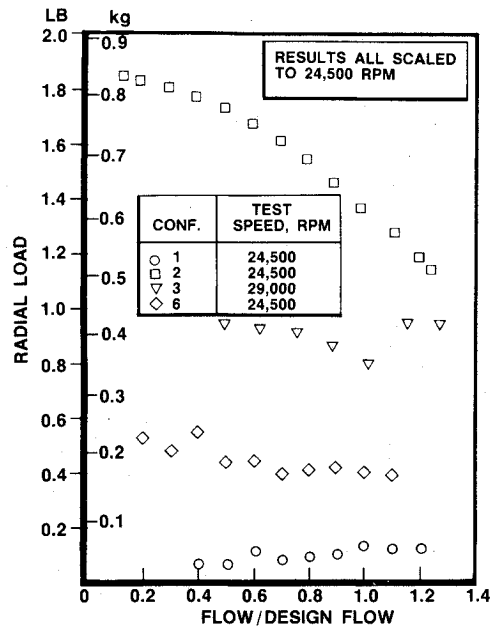

Fig. 15 Low-thrust pump, shrouded impellers (radial loads).

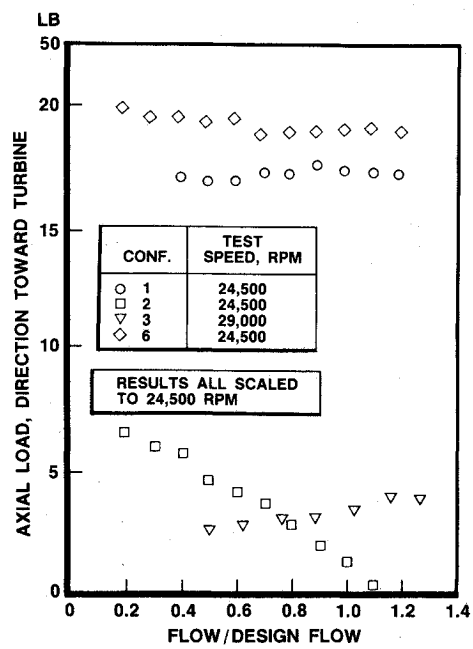

Fig. 16 Low-thrust pump, shrouded impellers (axial loads).

therefore the number of static pressure taps, depends on the configuration. For volute pumps, four taps are located equally spaced in the volute. From these pressures the static pressure at the impeller tip is determined by assuming a free vortex flow from the impeller discharge diameter to the pressure tap location.

Using the pressures at the impeller tip and assuming that the pressure distribution is linear between pressure taps, the incremental forces may be calculated. The resultant force is found by summing force components vectorially.

In all cases, the radial load is less than predicted by procedures presented by Stepanoff.[7] The design point test data are in the range of 8–68% of the predicted radial load. Test data plots of radial load vs flow/design flow are shown in Fig. 15.

Table 5 Diffusion system performance

Configuration	Impeller static head rise H_{imp}, m (ft)	Overall pump static head rise H_{ov}, m (ft)	Design point diffuser static head rise H_{dp} m (ft)	H_{dp}/H_{ov}
1	189 (620)	221 (724)	32(104)	0.14
2	176 (576)	229 (752)	54 (176)	0.23
3[a]	219 (720)	245 (805)	26 (85)	0.11
4	108 (354)	134 (440)	26 (86)	0.20
5[a]	59 (192)	74 (243)	16 (51)	0.21
6	193 (638)	227 (744)	22 (106)	0.14

[a]Test speed 29,000 rpm, results scaled to 24,500 rpm: $H_{dp} = H_{ov} - H_{imp}$

The two pumps showing the smallest radial loads are configurations 1 and 6. Both of these configurations have vaned diffusers. The only other pump with a vaned diffuser configuration 3 showed larger radial loads than configurations 1 and 6. However, the radial loads for configuration 3 were calculated using only the two diffuser inlet pressure taps and therefore are not as accurate as the other results. The vaned diffuser configurations exhibit radial loads that do not depend strongly on flow rate. This contrasts with the single discharge volute pumps, which show higher radial loads with a large dependence on flow rate. These characteristics agree with those predicted for the vaned diffuser and volute pumps. Vaned diffuser pumps are more desirable when wide flow range operation is required and a single discharge volute is specified.

Axial Loads

The axial load is determined from the static pressure distribution on the front and rear impeller face and by the impeller inlet pressure. The front face has three static pressure taps located at the shroud hub, midpoint, and tip. The rear face has two static pressure taps located at the shroud hub and tip.

The axial load vs flow/design flow is plotted in Fig. 16. The shrouded impellers show design point axial loads in the range of 1.2 kg (2.6 lb) to 19.2 kg (42.5 lb) in a direction toward the turbine. All axial and radial loads are well within bearing load capability in the design flow region. With vaned diffusers, load margins exist over a very wide flow range.

Conclusions and Recommendations

Tests were successfully completed to evaluate centrifugal pumps operating at specific speeds and sizes well below those previously reported.[8] The tests demonstrate that successful pump operation is possible in the specific speed range from 0.079 (215) to 0.158 (430). At the lower specific speed range, a severe efficiency penalty occurs since the hydraulic output power is substantially lower than the parasitic power. This fact can result in substantial pump-to-pump performance variations due to normal manufacturing tolerances.

The partial-emission diffuser concept has demonstrated the ability to use one impeller to cover a wide flow range by merely changing diffusers. The partial-admission impeller concept resulted in low efficiency with an open-face impeller.

Open-face impellers resulted in low efficiency due to large axial-clearance-to-passage-height ratio. Control of axial clearance to the close tolerances required by small open-face impellers for good performance is very difficult for small low specific-speed pumps.

The maximum efficiency occurred for a volute-type pump (configuration 2). The simplicity resulting from the absence of a vaned diffuser makes this configuration highly desirable when the engine operation permits single point operation. Single point operation permits volute design for a minimum radial load. When wide flow range operation is required, a vaned diffuser is desired to produce a low radial load over a wide flow range such as that exhibited by configuration 1.

Suction performance was close to predicted values at around 2.927 (8000) to 4.02 (11,000) suction specific speed, while axial and radial loads were less than predicted. There appeared to be no difference in the ability to cast the two impeller tip widths, and the smallest—0.762 (0.030 in.)—does not appear to be a limit.

References

[1]Furst, R.B., "Interim Report Small Centrifugal Pumps for Low Thrust Rockets," CR-174-913, NAS3-23164, March 1986.

[2]Balje, O.E., *Turbomachines*, Wiley, New York, 1981.

[3]Knapp, R.T., "Centrifugal Pump Performance as Affected by Design Features," *Transactions of the ASME*, Vol. 63, 1941, pp. 251–260.

[4]Van Le, N, "Partial Flow Centrifugal Compressors," ASME Paper 61-WA-135, 1961.

[5]Young, W.E. and Due, H.F., "Investigation of Pressure Prediction Methods for Low-Flow Radial Impellers, Phase III," Pratt and Whitney Aircraft Div., United Aircraft Corp., West Palm Beach, FL, Rept. PWA FR-1761, Jan. 13, 1966.

[6]Wislicenus, G.F., *Fluid Mechanics of Turbomachinery*, Dover, New York, 1965.

[7]Stepanoff, A.J., *Centrifugal and Axial Flow Pumps*, Rev. ed., Wiley, New York, 1960.

[8]Karassik, I.J., Krutzsch, W.C., Fraser, W.H., and Messina, J.P., *Pump Handbook*, McGraw-Hill, 1976.